Synthesis and characterization of three new Cu(II) paddle-wheel compounds with 1,3-benzodioxole-5-carboxylic acid

Francisco Sánchez-Férez [a], Joan Soldevila-Sanmartín [a], José A. Ayllón [a], Teresa Calvet [b], Mercè Font-Bardia [c], Josefina Pons [a,*]

a Departament de Química, Universitat Autònoma de Barcelona, 08193-Bellaterra, Barcelona, Spain
b Mineralogia, Petrologia i Geologia Aplicada, Universitat de Barcelona, Martí i Franquès s/n, 08028 Barcelona, Spain
c Unitat de Difracció de Raig-X, Centres Científics i Tecnològics de la Universitat de Barcelona (CCiTUB), Universitat de Barcelona, Solé i Sabarís, 1-3, 08028 Barcelona, Spain

josefina.pons@uab.cat (J. Pons).

ABSTRACT:

Three different paddle wheel compounds have been synthesized, each one via a different synthetic pathway. The first method is the reaction of Cu(MeCO2)2 H2O with 1,3-benzodioxole-5-carboxylic acid (Piperonylic acid, HPip) in a MeOH solution, yielding [Cu(m-Pip)2(MeOH)]2 (1). The second method is the transformation of the heteroleptic core paddle-wheel compound [Cu(m-MeCO2)(m-Pip)(MeOH)]2 into the homoleptic core paddle-wheel [Cu(m-Pip)2(DMSO)]2 2DMSO (2). Lastly, the third method is the substitution of the solvent molecule (DMF) present in the molecular array [Cu(m-Pip)2(DMF)]2 by 2-benzylpyridine (2-Bzpy) ligand, resulting in [Cu(m-Pip)2(2-Bzpy)]2 2.5MeOH H2O (3a). All compounds are characterized via EA, PXRD, ATR-FTIR, Far-IR and UV–Vis spectroscopy. For all three compounds, the X-ray crystal structure has been determined and their extended structures are discussed. Finally, TG/ DTA measurements have been recorded.

..

1. INTRODUCTION

The study of the coordination chemistry of Cu(II) complexes with carboxylate groups has a great interest due to their labile nature and versatility. They can present different coordination modes towards Cu(II): monodentate; chelate; bridging in syn-syn, syn-anti and anti-anti conformations. Furthermore, Cu(II) ions with d9 electronic configuration show different coordination numbers and geometry, varying from tetrahedral to octahedral [1]. This versatility allows the use of these compounds for applications in many research fields, such as catalysis, molecular electronics, magnetism and gas storage [2].

An important family of Cu(II) carboxylate complexes show paddle- wheel like structure. As of today, there are more than 1400 crystal structures with [Cu2(R-COO)4] homoleptic core described in the literature [3]. Most of them have been obtained by reaction between the Cu(II) salts and the corresponding acid in different solvents. An interesting topic is the analysis of its supramolecular scaffold, driven by nonbonding interactions. Therefore, its better understanding is one of the pillars of material design. In this sense, the substitution of the apical sites by auxiliary ligands promoting different supramolecular interactions leads to new architectures [4]. Within this framework, not only are discussed strong hydrogen bonds, but also new demonstrated significant interactions such as CAH□ □ □ O [5] and CAH□ □ □ g [6].

For instance, 1,3-benzodioxole-5-carboxylic acid (Piperonylic acid, HPip), containing a phenyl group and a dioxole ring, could promote the above-mentioned interactions. In addition, it is a natural molecule that exhibits biological activity such as: inhibition of certain enzymes (tyrosinase [7] and cinnamate 4-hydroxylase [8]), or stimulation of others (keratinocyte growth [9]).

Recently, our group has reported the preparation of Cu(II) and Zn(II) paddle-wheel compounds. They were obtained by reaction of M(MeCO2)2□ H2O (M = Zn(II), Cu(II)), HPip and pyridines. The synthesis of Zn(II) paddle-wheels was done using 3-phenylpyridine and 4-phenylpyridine as auxiliary ligands [10], whereas for Cu(II) paddle-wheels, 3-phenylpyridine and 4-benzylpyridine were used [11]. In addition, the reaction of Cu(MeCO2)2□ H2O with five pyridines (3-phenylpyridine, 2-benzylpyridine, 4-acetylpyridine [4b], 4-phenylpyridine [12] and 4-benzylpyridine [13]) resulted in the isolation of five new paddle-wheel compounds of general formula [Cu(MeCO2)2(dPy)]2.

We have also reported the reaction of [Cu(m-MeCO2)(m-Pip) (MeOH)]2 [14] with HPip and N,N-dimethylformamide (DMF) as solvent under reflux conditions, leading to the formation of [Cu(m-Pip)2(DMF)]2□ 2DMF [15]. Moreover, the reaction of [Cu(m-MeCO2) (m-Pip)(MeOH)]2 in presence of HPip and 2-benzylpyridine (2-Bzpy) in DMF as solvent yields [Cu(m-Pip)2(2-Bzpy)]2 [15].

There is not a standardised synthetic method leading to the formation of paddle-wheels. Therefore, compounds which already possess this structural motif could be used as reactants provided their core remains unaltered after the substitution. In this manuscript, we present three different synthetic methods for the obtaining of Cu(II) paddle-wheel compounds (Scheme 1). These methods are: (i) reaction between Cu(MeCO2)2□ H2O and HPip, (ii) transformation of the heteroleptic core paddle-wheel

compound [Cu(m-MeCO2)(m-Pip)(MeOH)]2 into the homoleptic one in presence of HPip ligand and (iii) by substitution of the apical solvent molecules (DMF) in [Cu(m-Pip)2(DMF)]2 2DMF for 2-Bzpy. As a result, the paddle-wheel compounds [Cu(m-Pip)2(MeOH)]2 (1) [Cu(m-Pip)2 (DMSO)]2 2DMSO (2) (DMSO = dimethyl sulfoxide) and [Cu(m-Pip)2(2-Bzpy)]2 2.5MeOH H2O (3a), were obtained via methods i, ii and iii, respectively.

The compounds were characterized by elemental analysis (EA), powder X-ray diffraction (PXRD), Attenuated Total Reflectance – Fourier Transformation Infrared spectroscopy (ATR-FTIR), Far-Infrared spectroscopy (FIR), Ultraviolet–Visible (UV–Vis) spectroscopy and single crystal X-ray diffraction method. Furthermore, its supramolecular networks were studied, regarding their potential applications in catalysis and gas storage/separation [16]. Finally, simultaneous TG/DTA determinations were performed to evaluate the thermal stability of the compounds.

2. RESULTS AND DISCUSSION

2.1. Synthesis and general characterization

Complex 1 was prepared by reaction of Cu(MeCO2)2 H2O and HPip in presence of 3,5-dimethyl-1-(2-hydroxyethyl)pyrazole [17] in MeOH solvent at r.t. This results in the formation of the homoleptic compound, with MeOH in the apical positions. For the obtaining of complex 2, compound [Cu(m-MeCO2)(m-Pip)(MeOH)2] [14] is refluxed in DMSO with stoichiometric amounts of HPip. As a result, the acetate ligands are displaced, whereas the Pip moieties do not only remain coordinated but also a further two other Pip moieties coordinate to the metal centre, obtaining an homoleptic core paddle-wheel compound with DMSO molecules in apical positions and two occluded DMSO molecules. Complex 3a was prepared by reaction of [Cu(l-Pip)2(DMF)]2 2DMF [15] with an excess of 2-benzylpyridine (2-Bzpy) in a MeOH solution under reflux conditions. This compound maintains its paddle-wheel structure, and the apical DMF molecules are replaced by 2-Bzpy moieties. Our research group has previously reported the synthesis of [Cu(l-Pip)2(2-Bzpy)]2 compound via two different methods [15]. Herein, reaction has been performed with an excess of 2-Bzpy ligand leading to compound 3a, which unlike the previous one, contains occluded solvent molecules (2.5 MeOH, H2O).

All compounds were characterized by EA, PXRD, ATR-FTIR, FIR and UV–Vis spectroscopy; and single crystal X-ray diffraction method. In addition, thermal stability was evaluated by TG/DTA determinations. Elemental analyses for compounds 1 and 2 agree with the proposed formula. For compound 3a, elemental analyses are in accordance with formula [Cu(m-Pip)2(2-Bzpy)]2 (3b) due to the loss of solvent molecules (2.5 MeOH and H2O). Phase purity of the sample was confirmed for compounds 1 and 2 (S.I.: Figs. S1–S2). For compound 3, the PXRD of the aerated sample denotes that the initial crystal structure has been modified (S.I.: Fig. S3). Under air exposure, the guest solvent is lost, as indicated by elemental analysis results.

The ATR-FTIR spectra of compounds 1–3 display the characteristic carboxylate bands in the range 1599–1582 cm 1 for mas(COO) and 1437–1435 cm 1 for ms(COO). The difference between these bands [D = mas(COO) ms(COO)] [18] for compounds 1–3 is 145, 156 and 164 cm 1, respectively, suggesting a bridging coordination mode for the carboxylate ligand (S.I.: Figs. S4–S6, respectively). The bands attributable to the aromatic groups [m(C@C), m(C@N)]ar, d (CAH)ip and d(CAH)oop are also present [19].

The presence of solvent molecules allows further identification of some specific bands. Compound 1, shows a broad band between 3424–3384 cm 1, attributable to m(OAH)MeOH. For compound 2, bands attributable to m(S@O) are observed, one at 1014 cm 1 attributable to free DMSO and the other at 1006 cm 1 belonging to coordinated DMSO. Furthermore, bands attributable to the m (CAS) vibration appear at 719 and 710 cm 1 [20]. Finally, for compound 3a, the band attributable to m(OH)MeOH+water appears at 3300 cm 1 [19].

In the Far IR region (500–400 cm 1) of compounds 1–3b, two well defined bands are observed. These bands are attributable to mas(CuAO) at 468 cm 1 and 458 cm 1 for 1; 464 cm 1 and 458 cm 1 for 2; and 468 cm 1 for 3b). For compound 3b, the mas(CuAN) is also observed at 424 cm 1 (S.I.: Fig. S7) [18].

The UV–Vis spectrum of compound 1 has not been recorded due to its insolubility in common solvents. The electronic spectra of compounds 2 and 3 have been recorded in DMSO as solvent. All spectra show one band in the visible region, characteristic of d9 Cu(II) complexes (S.I.: Fig. S8). Compound 2 has its kmax at 710 nm (Ɛ = 79M 1 cm 1) while 3 displayed the single band at 692 nm (Ɛ = 84M 1 cm 1). Therefore, the ATR-FTIR, Far-IR and UV–Vis spectral data, agree with the structures determined by single crystal X-ray diffraction.

2.2. Crystal structure of compounds 1–3a

Compounds 1–3a crystallize in the triclinic P 1 space group. The three compounds have a paddle-wheel binuclear Cu(II) structure with four bridging carboxylate ligands in a syn-syn coordination mode (Figs. 1–3). In compound 3a two crystallographically independent dimeric molecules (A and B) are present in the unit cell.

For 1 and 2, each Cu(II) metal atom is coordinated to five oxygen atoms. Four of them belong to the carboxylate group of Pip ligands, which are in the equatorial positions. The fifth one corresponds to the MeOH molecules in 1 and to the DMSO in 2. On the other hand, 3a shows a different coordination environment, including four oxygens from two Pip carboxylate groups in the equatorial position, but the apical position is occupied by a nitrogen atom belonging to the 2-Bzpy molecule instead of an oxygen atom.

In the equatorial plane the CuAOcarbox bond distances range from 1.943(5) to 1.976(5) Å, and the OACuAO(eq) angles between 87.37(5) and 91.51(5) . In the apical position, the value of CuAOMeOH (1), CuAODMSO (2) and CuAN2-Bzpy bond lengths are larger: 2.140(5) Å (1), 2.1417(12) Å (2) and 2.237(5) Å (molecule A), 2.250(5) Å (molecule B) (3a). In all three compounds each Cu(II) ion has a distorted square-pyramidal geometry (s = 0.005 (1); 0.002 (2) and 0.006 molecule A, and 0.004 molecule B (3a)) [21]. This distortion is subtly exhibited in the angles between the equatorial planes and the apical position, which show a small deviation for 1 and 2 (OcarboxACuAOMeOH 93.3(2)–98.30(19) (1), OcarboxACuAODMSO 94.99(3)–96.13(7) (2)) and a bigger one for 3a (OcarboxACuAN2-Bzpy 92.79(19)–99.30(19) (molecule A) and 91.7(2)–100.5(2) (molecule B)), taking into account that the perfect angle is 90 .

Finally, in the three structures, Cu(II) ions are displaced from the basal plane (0.197 Å (1); 0.192 Å (2) and 0.206 Å (molecule A) 0.208 Å (molecule B) (3a)) towards the apical position.

The intermolecular Cu Cu distances are 2.5907(17) Å (1), 2.6357(4) Å (2) and 2.6573(15) Å (molecule A), 2.6647(15) Å (molecule B) (3a), which are similar to values previously reported in the literature (2.58–2.76 Å) [22].

Selected distances and angles for 1–3a are provided in Tables 1–3, respectively.

2.3. Extended structures of 1–3a

For compounds 1 and 2, 2D layers parallel to the ab plane are formed by the expansion of intermolecular interactions in which both ligands and solvent molecules participate (Figs. 4a, 5a). In the case of 1, coordinated MeOH molecules interact with the neighbouring dimeric units by the coordinated carboxylate oxygen of a Pip unit and forms 1D chains along the a axis (Fig. 4b). In parallel, the aliphatic carbon atoms of the dioxole ring, interact with the aromatic ring of a Pip ligand via CAH□ □ □ g interaction [6] along the b axis (Fig. 4c).

In 2 the intermolecular interactions are mainly driven via occluded DMSO molecules. Two simultaneous hydrogen bond interactions involving the uncoordinated DMSO molecules generate 1D chains along the a axis (Fig. 5b). The oxygen atom of the sulfoxide group interacts with the aliphatic carbon of a Pip ligand and in turn, with the methyl group of a coordinated DMSO molecule. Finally, the b axis expansion is supported by a CorthoAH□ □ □ O interaction [5] between two Pip units (Fig. 5c). In compound 3a the supramolecular net is only based on a CorthoAH□ □ □ g interaction [6] involving two Pip ligands and a weak g–g interaction between the pyridil rings of the 2-Bzpy units (Fig. 6a). The compound includes solvent occluded molecules that do not exhibit strong interactions with the supramolecular network (Fig. 6b). The space occupied by these solvent molecules generates a solvent accessible volume of 205.33 Å3 (7.1% of the cell volume). Under air exposure, the guest solvent is lost, as indicated by elemental analysis results. Unfortunately, these changes seem to provoke the collapse of the pores, and the material does not readsorb the withdrawn solvent molecules. Relevant intermolecular interactions of the compounds 1-3a are summarized in Table 4.

2.4. Thermogravimetric analysis

Simultaneous TG-DTA determinations were carried out to evaluate for the thermal stability of compounds 1–3. The measurements were performed using 52.2 mg of 1, 54.2 mg of 2 and 60.2 mg of 3. Compound 1 starts to lose the first coordinated MeOH molecule at 65 □ C (weight loss exp. 4.4%, calc. 3.7%). The second weight loss occurs between 119 □ C and 251 □ C and can be attributed to the loss of the remaining MeOH molecule (weight loss exp. 2.6%, calc. 3.7%). The more important step is an overlapped process that occurs between 251 □ C and 320 □ C with 37.1% weight loss relative to coordinated Pip ligands (calc. 38.8%) (S.I.: Fig. S9).

For compound 2 the first step appears between 105 □ C and 188 □ C and can be assigned to the loss of three DMSO molecules, two lattice and one coordinated (weight loss exp. 19.8%, calc. 21.3%). As a follow-up there is the loss of the remaining coordinated DMSO molecule between 188 and 245 □ C (weight loss exp. 6.8%, calc. 7.1%). From this temperature, the compound continues its decomposition ending at 304 □ C (S.I.: Fig. S10).

As mentioned before, compound 3a unavoidably loses the solvent occluded molecules before the experiment yielding compound 3b. Compound 3b decomposition shows only one major step of mass loss (weight loss exp. 40.5%) between 166 °C and 269 °C. No thermal events assignable to the solvent molecules have been observed, confirming the loss of solvent molecules under air exposure (SI: Fig. S11).

3. CONCLUSIONS

In summary, we have presented the synthesis and characterization of three new paddle-wheel complexes. These compounds were obtained via three different methods: reaction, homoleptic to heteroleptic core transformation and coordinated solvent substitution. These compounds have been fully characterized to investigate its preparation and structural properties. The crystal structure confirmed that all of them exhibited four bridged Pip ligands in a syn-syn coordination mode. Two of these compounds (1, 2) have solvent molecules occupying the apical positions while in 3 this position is occupied by the 2-benzylpyridine. Besides, their extended structures have been studied yielding 2D (1, 2) and 1D (3a) networks. In addition, their thermal stability was analysed by TG/DTA. The loss of uncoordinated and coordinated solvent molecules (MeOH, 1; DMSO, 2) was observed followed onwards by decomposition between 251 °C and 245 °C. Compound 3 decomposes without thermal events assignable to the solvent molecules, so the analysed sample corresponds to 3b compound.

4. EXPERIMENTAL

4.1. Materials and general details

Cu(II) acetate monohydrate (Cu(MeCO2)2 H2O), 1,3-benzodioxole-5-carboxylic acid (piperonylic acid, HPip) and 2-benzylpyridine (2-Bzpy) ligands, methanol (MeOH) and dimethylformamide (DMF), were purchased from Sigma-Aldrich and used without further purification. All reactions and manipulation were carried out in air. Elemental analyses (C, H, N) were carried out by the staff of Chemical Analysis Service of the Universitat de Barcelona on a Thermo Scientific Flash 2000 CHNS Analyses. Powder X-ray diffraction (PXRD) patterns were measured with a Siemens D5000 apparatus (with 40 kW and 45 mA using Cu Ka radiation with k = 1.5406 Å). All of them were recorded from 2b = 5–30 with a step scan of 0.02 counting 1 s each step. ATR-FTIR spectra were recorded at the Chemical Analysis Service of the Universitat Autònoma de Barcelona on a Tensor 27 (Bruker) spectrometer, equipped with an attenuated total reflectance (ATR) accessory model MKII Golden Gate with diamond window in the range 4000–600 cm 1. Far-IR spectra were recorded on a Perkin Elmer spectrometer, equipped with a universal attenuated total reflectance (ATR) accessory with a diamond window in the range 600–400 cm 1. The electronic spectra in solution of DMSO (1 10 3 M) were run on a Agilent HP 8453 UV–Vis spectrophotometer with a quartz cell having a path length of 1 cmin the range of 500–800 nm. Simultaneous TG/DTA determinations were carried out in a Netzsch STA 409 instrument, with an aluminium oxide powder (Al2O3) crucible and heating at 5 C min 1 from 25 to 400 C, under a nitrogen atmosphere with a flow rate of 80 mL min 1. Al2 O3 (Perkin–Elmer 0419-0197) was used as Standard. Compounds [Cu(m-MeCO2)(m-Pip)(MeOH)]2 [14] and [Cu(m-Pip)2(DMF)]2 2DMF [15] were previously synthesized in our research group and 1-(2-hydroxyethyl)-3,5-dimethylpyrazole was synthesized as described in the literature [17].

4.2. Synthesis of the compound [Cu(m-Pip)2(MeOH)]2 (1)

To a solution of Cu(MeCO2)2 H2O (20.0 mg, 1.0 mmol) in MeOH (20 mL) a solution of HPip (34.0 mg, 2.0 mmol) and 1-(2-hydroxyethyl)-3,5-dimethylpyrazole (28.0 mg, 2.0 mmol) in MeOH (20 mL) was added dropwise. The green solution was evaporated at r.t. until green crystals were obtained after 22 days. Yield: 35.7 mg (42%). Anal. Calc. for C34H28Cu2O18 (851.67 gmol 1): C, 47.95; H, 3.31. Found: C, 47.83; H, 3.24%. ATR-FTIR (wavenumber, cm 1): 3424–3384(br) [m(OH)]MeOH, 3096(w) [m(CH)]ar, 3057(w) [m(CH)]ar, 2904(w) [m(CH)] al, 2880(w) [m(CH)] al, 1628(w), 1582(m) [mas(COO)], 1504(w) [m(C@C), m(C@N)], 1490 (w), 1437(s) [ms(COO)], 1381(s) [d(C@C), d(C@N)], 1248(m), 1172 (w), 1113(m) [m(CAOAC)], 1081(w), 1037(s), 1026(s) [dip(CAH)], 938 (m), 922(m), 892(w), 834(w), 804(m), 775(s) [doop(CAH)], 723(m), 684(s), 586(s).

4.3. Synthesis of the compound [Cu(m-Pip)2(DMSO)]2 2DMSO (2)

To a colourless solution of HPip (51.9 mg; 0.313 mmol) in DMSO (15 mL), a green solution of [Cu(m-MeCO2)(m-Pip)(MeOH)]2 (100 mg, 0.157 mmol) in DMSO (15 mL) was added and stirred under reflux conditions for 24 h. The solution was vacuumed until half of the volume. The blue crystalline solid appears. The compound was filtered, washed with 10 mL of cold diethylether and dried on air. Suitable blue crystals were obtained after evaporation of the mother liquors in air for three days. Yield: 101.9 mg (74%). Anal. Calc. for C40H44Cu2O20S4 (1100.10 gmol 1): C, 43.67; H, 4.03; S, 11.66. Found: C, 43.52; H, 3.98; S, 11.48 %. ATR-FTIR (wavenumber, cm 1): 3014(w) [m(CH)]ar, 2913(w) [m(CH)] al, 1633(m), 1593(s) [mas(COO)], 1503(m) [m(C@C), m(C@N)], 1488(m), 1437(s) [ms(COO)], 1408(m), 1384(s) [d(C@C), d (C@N)], 1357(s), 1310(m), 1286(w), 1257(s), 1240(s), 1170(m), 1112(m) [m(CAOAC)], 1078(w), 1055(m), 1027(s) [dip(CAH)], 1014(s) [m(SO)]free, 1006(s) [m(SO)]coord, 936 (w), 917(s), 885(m), 840(w), 817(w), 804(s), 770(s) [doop(CAH)], 719(m), 710(w) [mas(CAS)], 680(s), 608(m), 585(s), 519(w).

4.4. Synthesis of the compound [Cu(m-Pip)2(2-Bzpy)]2 2.5 MeOH H2O (3a)

To a green solution of [Cu(m-Pip)2(DMF)]2 2DMF (100 mg, 0.093 mmol) in MeOH (25 mL), a yellowish solution of 2-Bzpy (0.60 mL, 0.372 mmol) in MeOH (5 mL) was added and stirred under reflux conditions for 24 h. The green solution was treated with sequential cooling evaporation cycles and a green precipitate was formed. The compound was filtered, washed with 10 mL of cold MeOH and dried on air. Suitable green crystals were obtained after evaporation of the mother liquors in air for ten days. The stoichiometry of this compound was definitely established after determination of their X-ray crystal structure. However, the occluded solvent molecules are withdrawn from the structure after manipulation required for preparing the sample for EA yielding [Cu (m-Pip)2(2-Bzpy)]2 (3b).

Yield: 50.1 mg (46%). Anal. Calc. for C114.5H96Cu4O35.5N4 (2344.18 gmol 1). ATR-FTIR (wavenumber, cm 1): 3300(m) [m(OH)]MeOH+H2O, 3031(w) [m(CH)]ar, 3018(w) [m(CH)]ar, 2900(w) [m(CH)] al, 1633(m), 1612(m), 1599(s) [mas(COO)], 1569(m) [m (C@C), m(C@N)], 1496(m), 1486(m), 1473(w), 1435(s) [ms(COO], 1390(s) [d(C@C), d(C@N)], 1347(m), 1320(m), 1256(s), 1239(m), 1159(m), 1110(m) [m(CAOAC)], 1073(m), 1058(m), 1034(m) [dip(- CAH)], 1011(m), 995(m), 985(m), 936 (m), 923(m), 884(m), 805 (w), 774(m) [doop(CAH)], 776(m), 743(m), 722(m), 699(s), 681(s), 662(m), 652(m), 638(w), 618(s), 611(s), 596(m), 571(m), 564(s). 3b. Anal. Calc. for C112H81Cu4O32N4 (2249.02 gmol 1): C, 59.81; H, 3.63; N, 2.49. Found: C, 59.67; H, 3.58; N, 2.31%. ATR-FTIR (wavenumber, cm 1): 3082–3006(br) [m(CH)]ar, 2957–2870(br) [m (CH)] al, 1633(m), 1592(s) [mas(COO)], 1569(m) [m(C@C), m(C@N)], 1504(w), 1489(m), 1438(s) [ms(COO], 1385(s) [d(C@C), d(C@N)], 1256(s), 1240(m), 1169(m), 1112(m) [m(CAOAC)], 1076(m), 1034 (m) [dip(CAH)], 1011(m), 937 (m), 923(m), 874(m), 804(w), 771 (m) [doop(CAH)], 683(m).

4.5. X-ray crystallography

For compound 1 and 3a, a green and for 2 a blue prism-like specimen was used for the X-ray crystallographic analysis. The X-ray intensity data were measured on a D8 Venture system equipped with a multilayer mono-chromate and a Mo microfocus (k = 0.71073 Å). For 1-3a, the frames were integrated with the Bruker SAINT Software package using a narrow-frame algorithm. For 1, the integration of the data using a triclinic unit cell yielded a total of 6740 reflections to a maxim h angle of 23.31 (0.90 Å resolution), of which 2312 were independent (average redundancy 2.915, completeness = 95.1%), Rint = 10.19%, Rsig = 11.29%) and 1510 (65.31%) were greater than 2r(F2). The calculated minimum and maximum transmission coefficients (based on crystal size) are 0.6029 and 0.7449. For 2, the integration of the data using a triclinic unit cell yielded a total of 42,882 reflections to a maxim h angle of 31.58 (0.68 Å resolution), of which 7357 were independent (average redundancy 5.829, completeness = 99.6%), Rint = 4.40%, Rsig = 3.89%) and 5906 (80.28%) were greater than 2r(F2). The calculated minimum and maximum transmission coefficients (based on crystal size) are 0.6941 and 0.7462. For 3a, the integration of the data using a triclinic unit cell yielded a total of 76,010 reflections to a maxim h angle of 23.94 (0.88 Å resolution), of which 8998 were independent (average redundancy 8.447, completeness = 99.5%), Rint = 9.29%, Rsig = 5.08%) and 5978 (66.44%) were greater than 2r (F2). The calculated minimum and maximum transmission coefficients (based on crystal size) are 0.6700 and 0.7450.

The structures were solved using the Bruker SHELXTL Software, package and refined using SHELX (version-2018/3) [23]. For 1, the final anisotropic full-matrix least-squares refinement on F2 with 244 variables converged at R1 = 5.75%, for the observed data and wR2 = 14.29% for all data. For 2, the final anisotropic full-matrix least-squares refinement on F2 with 302 variables converged at R1 = 3.53%, for the observed data and wR2 = 7.77% for all data. For 3a, the final anisotropic full-matrix least-squares refinement on F2 with 727 variables converged at R1 = 7.37%, for the observed data and wR2 = 22.56% for all data. For 1–3a, the final cell constants and volume, are based upon the refinement of the XYZ-centroids of reflections above 20 r(I). Data were corrected for absorption effects using the multi-scan method (SADABS). Crystal data and relevant details of structure refinement for compounds 1–3a, are reported in Table 5. Molecular graphics were generated with the program MERCURY 3.6 [24] Color codes for all molecular graphics: blue (Cu), light blue (N), red (O), grey (C), white (H).

ACKNOWLEDGEMENTS

This work was financed by the CB615921 project and the Spanish National Plan of Research MAT2015-65756R and 2017SGR1687 project from the Generalitat de Catalunya.

REFERENCES

[1] (a) F.P.W. Agterberg, H.A.J. Kluit, W.L. Driessen, H. Oevering, W. Buijs, M.T. Lakin, A.L. Spek, J. Reedijk, Inorg. Chem. 36 (1997) 4321; (b) J.M. Rueff, N. Masciocchi, P. Rabu, A. Sironi, A. Skoulios, Eur. J. Inorg. Chem. (2001) 2843; (c) R.L. Rardin, A. Bino, P. Poganiuch, W.B. Tolman, S. Liu, S.J. Lippard, Angew. Chem., Int. Ed. Engl. 102 (1990) 842; (d) R.P. Sharma, A. Saini, J. Kumar, S. Kumar, P. Venugopalan, V. Ferretti, Inorg. Chim. Acta 457 (2017) 59.

[2] (a) N. Abdullah, Y. Al-Hakem, N. Abdullah, H. Samsudin, N.S.A. Tajidi, Asian. J Chem. 26 (2014) 987; (b) V. Paredes-García, R.C. Santana, R. Madrid, A. Vega, E. Spodine, D. Venegas-Yazigi, Inorg. Chem. 52 (2013) 8369; (c) C. Sanchez, K.J. Shea, S. Kitagawa, Chem. Soc. Rev. 40 (2011) 471; (d) Y. Xie, H. Yang, Z.U. Wang, Y. Liu, H.C. Zhou, J.-R. Li, Chemm. Commun. 50 (2014) 563; (e) C.-S. Liu, J.-J. Wang, L.-F. Yan, Z. Dhang, X.-H. Bu, E.C. Sañudo, J. Ribas, Inorg. Chem. 46 (2007) 6299.

[3] C.R. Groom, I.J. Bruno, M.P. Lightfoot, S.C. Ward, Acta Crystallogr. Sect B Struct. Sci. Cryst. Eng. Mater. 72 (2016) 171.

[4] (a) G. Beobide, O. Castillo, A. Luque, S. Pérez-Yáñez, CrystEngComm 17 (2015) 3051; (b) M. Guerrero, J.A. Ayllón, T. Calvet, M. Font-Bardía, J. Pons, Polyhedron 134 (2017) 107.

[5] T. Steiner, W. Saenger, J. Am. Chem. Soc. 114 (1992) 10146.

[6] S. Tsuzuki, Annu. Rep. Prog. Chem., Sect. C: Phys. Chem. 108 (2012) 69.

[7] Y.-X. Si, S. Ji, N.-Y. Fang, W. Wang, J.-M. Yang, G.-Y. Qian, Y.-D. Park, J. Lee, S.-J. Yin, Process Biochem. 48 (2013) 1706.

[8] V.H. Salvador, R.B. Lima, W.D. Dos Santos, A.R. Soares, P.A.F. Böhm, R. Marchiosi, M.de L.L. Ferrarese, O. Ferrarese-Filho, PLoS One 8 (2013) e69105.

[9] D. Lee, J. Lim, K.-C. Woo, K.-T. Kim, Sci. Rep. 8 (2018) 162.

[10] M. Guerrero, S. Vázquez, J.A. Ayllón, T. Calvet, M. Font-Bardía, J. Pons, ChemistrySelect 2 (2017) 632.

[11] J. Soldevila-Sanmartín, J.A. Ayllón, T. Calvet, M. Font-Bardía, J. Pons, Polyhedron 126 (2017) 184.

[12] J. Soldevila-Sanmartín, J.A. Ayllón, T. Calvet, M. Font-Bardía, J. Pons, Polyhedron 135 (2017) 36.

[13] J. Soldevila-Sanmartín, M. Sanchez-Sala, T. Calvet, M. Font-Bardía, J.A. Ayllón, J. Pons, J. Mol. Struct. 1171 (2018) 808.

[14] J. Soldevila-Sanmartín, J.A. Ayllón, T. Calvet, M. Font-Bardía, C. Domingo, J. Pons, Inorg. Chem. Commun. 71 (2016) 90.

[15] F. Sánchez-Férez, M. Guerrero, J.A. Ayllón, T. Calvet, M. Font-Bardía, J. Giner Planas, J. Pons, Inorg. Chim. Acta 487 (2019) 295.

[16] (a) S. Galli, A. Maspero, C. Giacobbe, G. Palmisano, L. Nardo, A. Comotti, I. Bassanetti, P. Sozzani, N. Masciocchi, J. Mat. Chem. A 2 (2014) 12208; (b) A. Tabacaru, C. Pettinati, I. Tomokhin, F. Marchetti, F. Carrasco-Marín, F.J. Maldonado-Hodar, S. Galli, N. Masciocchi, Cryst. Grown Des. 13 (2013) 3087; (c) L.-Y. Du, W.-J. Shi, L. Hou, Y.-Y. Wang, Q.-Z. Shi, Z. Zhu, Inorg. Chem. 52 (2013) 14018; (d) V.V. Ponomarova, V.V. Komarchuk, I. Boldog, H. Krautscheid, K.V. Domasevitch, CrystEngComm 15 (2013) 8280; (e) C. Pettinati, A. Tabacaru, I. Boldog, K.V. Damasevitch, S. Galli, N. Masciocchi, Inorg. Chem. 51 (2012) 5235; (f) J.-P. Zhang, S. Kitagawa, J. Am. Chem. Soc. 130 (2008) 907; (g) Y. Chen, B. Wang, X. Wang, L.-H. Xie, J. Li, Y. Xie, J.-R. Li, A.C.S. Appl, Mater. Interfaces 9 (2017) 27027.

[17] W.G. Haanstra, J. Reedijk, J. Chem. Soc., Dalton Trans. (1989) 2309.

[18] (a) R.J. Deacon, G.B. Phyllips, Coord. Chem. Rev. 33 (1980) 227; (b) K. Nakamoto, Infrared and Raman Spectra of Inorganic and Coordination Compounds. Applications in Coordination, Organometallic, and Bioinorganic Chemistry, sixth ed., Wiley Interscience, New York, USA, 2009.

[19] D.H. Williams, I. Fleming, Spectroscopic Methods in Organic Chemistry, McGrawHill, London, UK, 1995.

[20] (a) W.R. Fawcett, A.A. Kloss, J. Phys. Chem. 100 (1996) 2019; (b) F.A. Cotton, R. Francis, W.D. Horrocks, J. Phys. Chem. 64 (1960) 1534.

[21] A.W. Addison, T.N. Rao, J. Chem. Soc., Dalton Trans. 1 (1984) 1349.

[22] (a) S. Gomathi, P.T. Mutthiah, Acta Crystallogr. C 69 (2011) 1498; (b) M. Barquín, N. Cocera, M.J. González-Garmendia, L. Larrínaga, E. Pinilla, M. R. Torres, J. Coord. Chem. 63 (2010)

2247; (c) A. Pichon, C.M. Fierro, M. Nieuwenhuyzen, L.J. Stuart, CrystEngComm 9 (2007) 449.

[23] G.M. Sheldrick, Acta Crystallogr. Sect. A Found. Crystallogr. 64 (2007) 112.

[24] (a) C.F. Macrae, P.R. Edgington, P. McCabe, E. Pidcock, G. Shields, R. Taylor, M. Towler, J.J. van de Streek, Appl. Crystallogr. 39 (2006) 453; (b) C.F. Macrae, I.J. Bruno, J.A. Chisholm, P.R. Edgington, P. McCabe, E. Pidcock, I. Rodriguez-Monge, R. Taylor, M. Towler, J. van de Streek, P.A.J. Wood, Appl. Crystallogr. 41 (2008) 466.

Legends to figures

Scheme 1. Schematic representation of the three different reactions.

Figure. 1. Molecular structure representation of compound 1. Hydrogen atoms are omitted for clarity except for MeOH molecules.

Figure. 2. Molecular structure representation of compound 2. Hydrogen atoms are omitted for clarity except for DMSO molecules.

Figure. 3. Molecular structure representation of compound 3a showing the two crystallographically independent units comprised in the unit cell (a. A, b. B). Hydrogen atoms are omitted for clarity.

Figure. 4. (a) Perpendicular view of the 2D layers generated by 1 along the ab plane. (b) a axis expansion through MeOH□ □ □ Pip interaction. (c) b axis expansion via CAH□ □ □ g interaction. Only hydrogen atoms involved in the intermolecular interactions are shown.

Figure. 5. (a) Perpendicular view of the 2D layers generated by 2 along the ab plane. (b) a axis expansion through CAH (Pip)□ □ □ O(Pip) interaction. (c) b axis expansion via simultaneous CAH(Pip)□ □ □ O(DMSO)/O(DMSO)□ □ □ HAC(DMSO) interaction. Only hydrogen atoms involved in the intermolecular interactions are shown.

Figure. 6. (a) ab view of the 1D chains present in 3a along the [1 0 □ 1] direction. (b) b axis view of the channelling generated by solvent occluded molecules (2.5MeOH and H2O).
Only hydrogen atoms involved in the intermolecular interactions are shown.

SCHEME 1

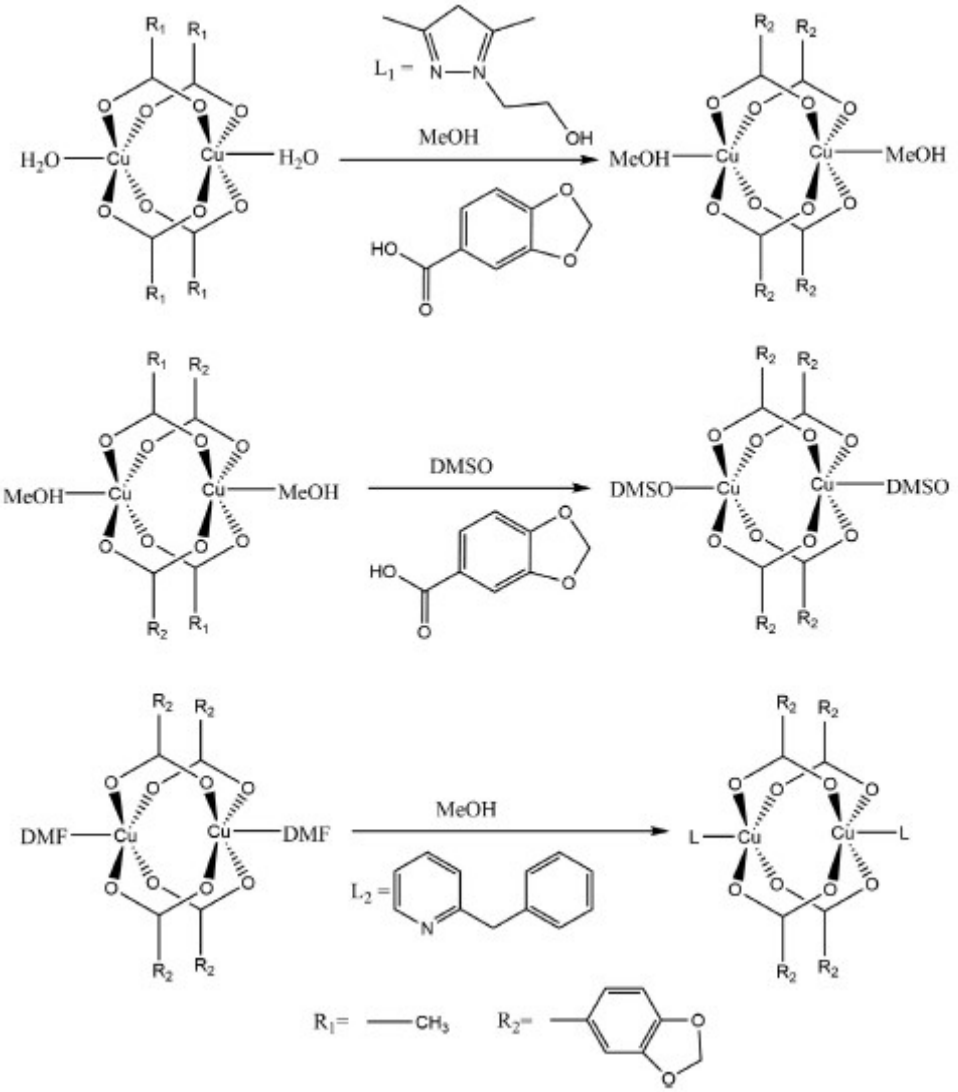

FIGURE 1

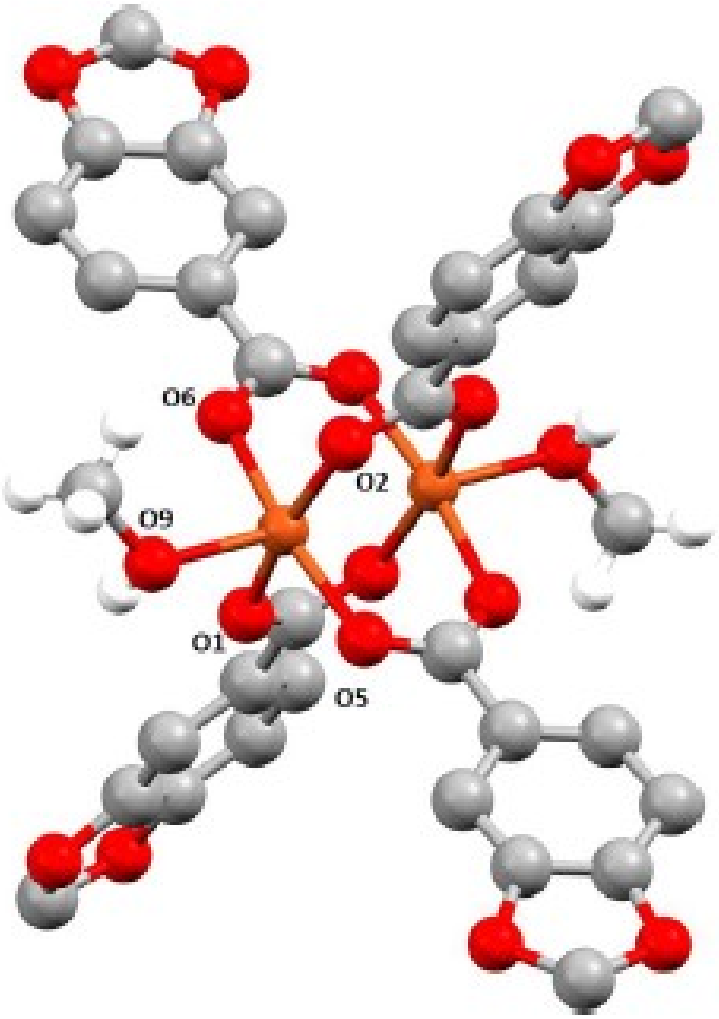

FIGURE 2

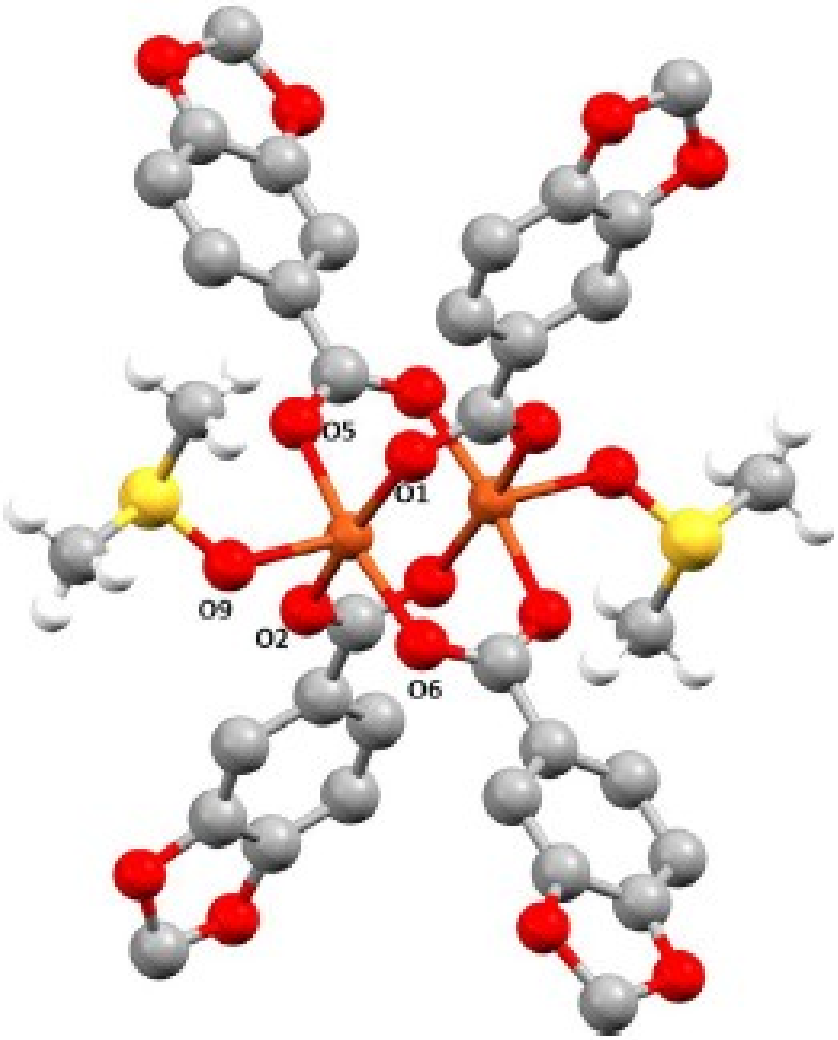

FIGURE 3

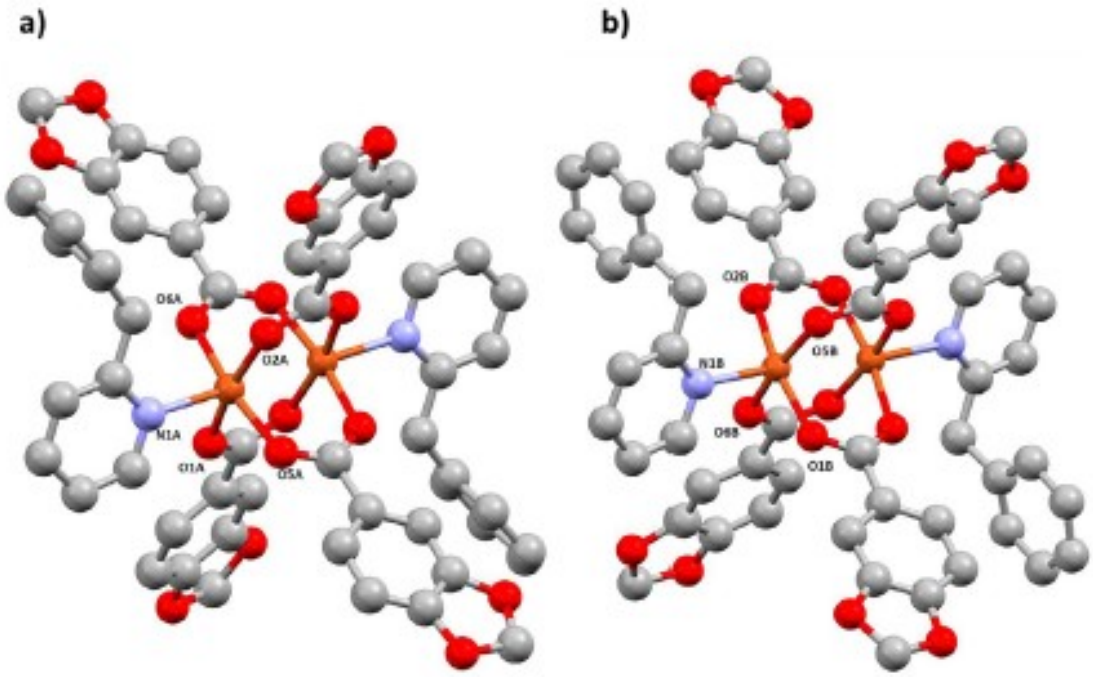

FIGURE 4

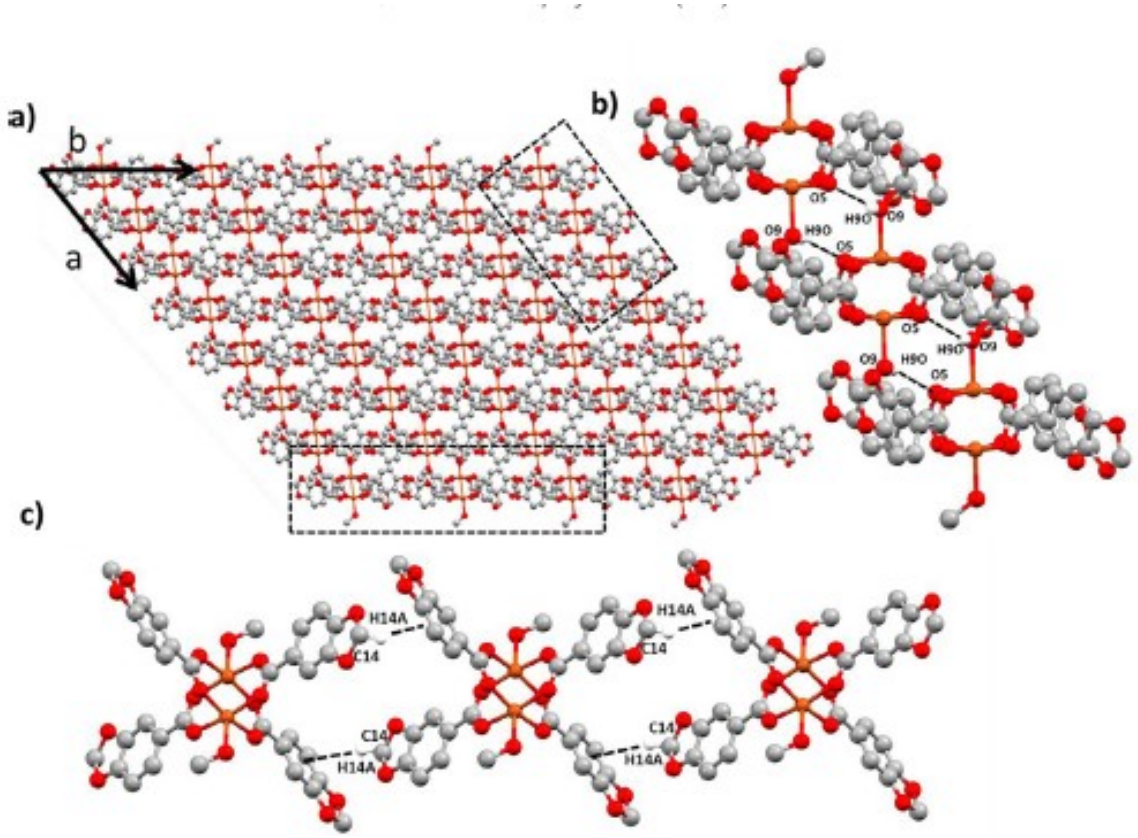

FIGURE 5

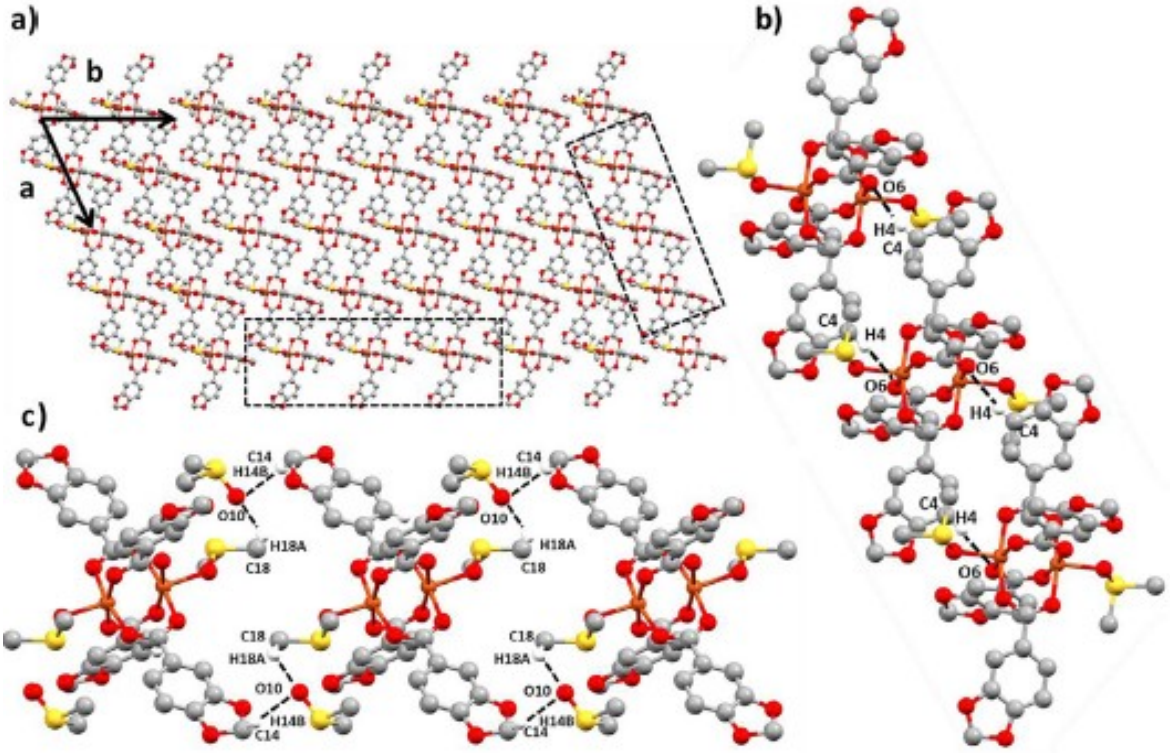

FIGURE 6

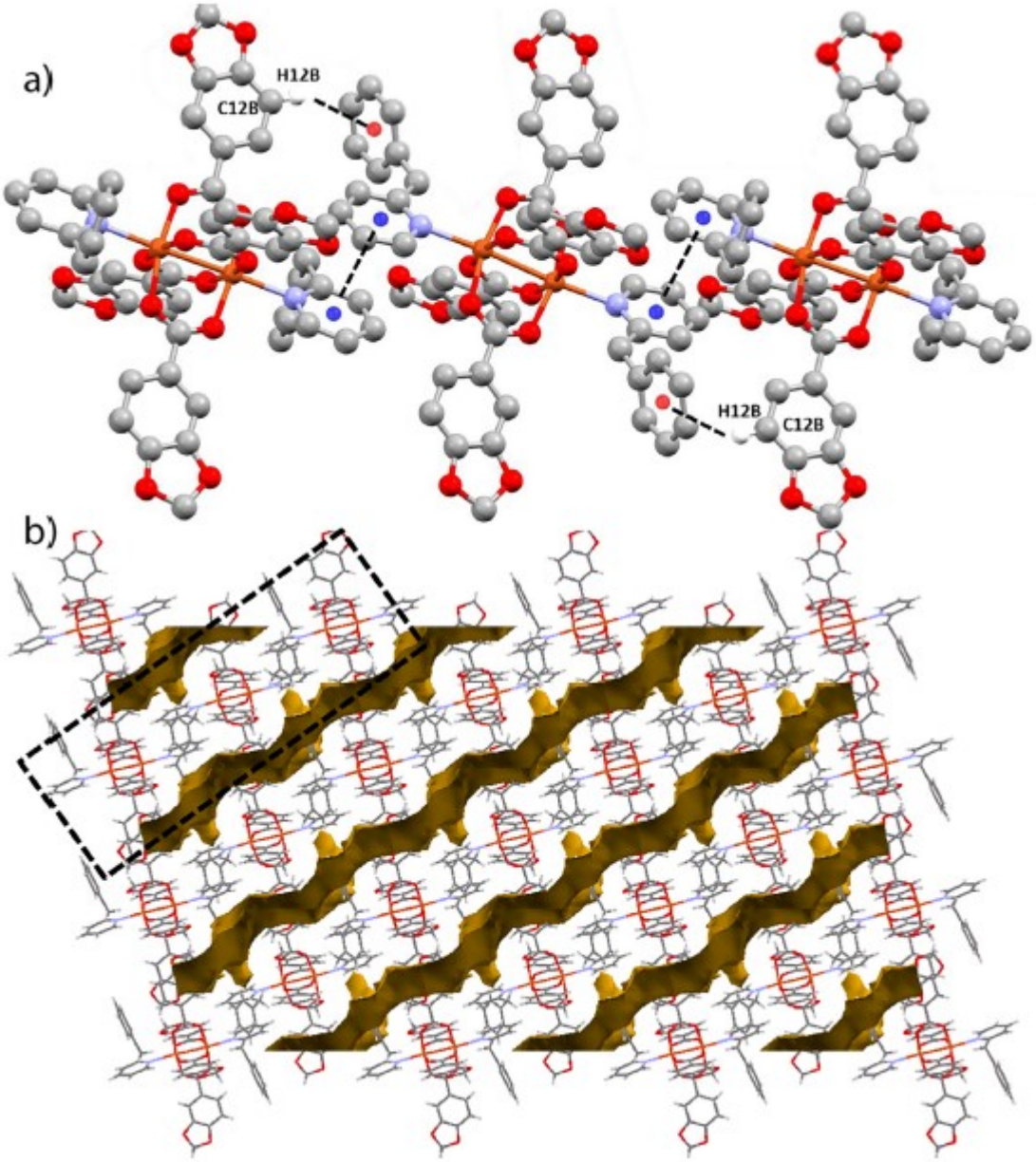

Table 1. Selected bond lengths (Å) and bond angles (°) for 1.

Bond length (Å)			
Cu(1)–O(2)#1	1.943(5)	Cu(1)–O(6)#1	1.957(5)
Cu(1)–O(1)	1.948(5)	Cu(1)–O(9)	2.140(5)
Cu(1)–O(5)	1.951(5)	Cu(1)–Cu(1)#1	2.591(2)
Bond angles (°)			
O(2)#1–Cu(1)–O(1)	168.3(2)	O(5)–Cu(1)–O(6)#1	168.3(2)
O(2)#1–Cu(1)–O(5)	89.2(3)	O(2)#1–Cu(1)–O(9)	98.30(19)
O(1)–Cu(1)–O(5)	87.6(3)	O(1)–Cu(1)–O(9)	93.3(2)
O(2)#1–Cu(1)– O(6)#1	91.0(2)	O(5)–Cu(1)–O(9)	97.3(2)
O(1)–Cu(1)– O(6)#1	89.9(3)	O(6)#1–Cu(1)–O(9)	94.26(19)

#1: 1 − x, −y + 1, −z + 1.

Table 2 . Selected bond lengths (Å) and bond angles (°) for 2.

Bond length (Å)			
Cu(1)–O(1)	1.9631(12)	Cu(1)–O(5)	1.9748(12)
Cu(1)–O(2)#1	1.9671(12)	Cu(1)–O(9)	2.1417(12)
Cu(1)–O(6)#1	1.9687(12)	Cu(1)–Cu(1)#1	2.6357(4)
Bond angles (°)			
O(1)–Cu(1)–O(2)#1	168.74(5)	O(6)#1–Cu(1)–O(5)	168.88(5)
O(1)–Cu(1)–O(6)#1	91.51(5)	O(1)–Cu(1)–O(9)	95.86(5)
O(2)#1–Cu(1)–O(6)#1	88.38(5)	O(2)#1–Cu(1)–O(9)	95.35(5)
O(1)–Cu(1)–O(5)	87.37(5)	O(6)#1–Cu(1)–O(9)	94.99(5)
O(2)#1–Cu(1)–O(5)	90.58(5)	O(5)–Cu(1)–O(9)	85.56(4)

#1: $-x+1, -y+1, -z+2$.

Table 3. Selected bond lengths (Å) and bond angles (°) for 3a.

Molecule A			
Bond length (Å)			
Cu(1A)–O(5A)	1.959(5)	Cu(1A)–O(1A)	1.975(5)
Cu(1A)–O(6A)#2	1.961(5)	Cu(1A)–N(1A)	2.237(5)
Cu(1A)–O(2A)#2	1.973(5)	Cu(1A)–Cu(1A)#2	2.6573(15)
Bond angles (°)			
O(5A)–Cu(1A)–O(6A)#2	168.0(2)	O(2A)#2–Cu(1A)–O(1A)	167.6(2)
O(5A)–Cu(1A)–O(2A)#2	88.5(2)	O(5A)–Cu(1A)–N(1A)	96.4(2)
O(6A)#2–Cu(1A)–O(2A)#2	90.7(2)	O(6A)#2–Cu(1A)–N(1A)	95.6(2)
O(5A)–Cu(1A)–O(1A)	87.5(2)	O(2A)#2–Cu(1A)–N(1A)	99.3(2)
O(6A)#2–Cu(1A)–O(1A)	90.7(2)	O(1A)–Cu(1A)–N(1A)	92.8(2)
Molecule B			
Cu(1B)–O(5B)	1.965(5)	Cu(1B)–O(1B)	1.976(5)
Cu(1B)–O(6B)#1	1.965(4)	Cu(1B)–N(1B)	2.250(5)
Cu(1A)–O(2B)#1	1.965(5)	Cu(1B)–Cu(1B)#1	2.665(2)
Bond angles (°)			
O(5B)–Cu(1B)–O(6B)#1	168.1(2)	O(2B)#1–Cu(1B)–O(1B)	167.8(2)
O(5B)–Cu(1B)–O(2B)#1	88.9(2)	O(5B)–Cu(1B)–N(1B)	100.0(2)
O(6B)#2–Cu(1B)–O(2B)#1	89.9(2)	O(6B)#1–Cu(1A)–N(1B)	91.9(2)
O(5B)–Cu(1B)–O(1B)	90.0(2)	O(2B)#1–Cu(1B)–N(1B)	100.5(2)
O(6B)#1–Cu(1B)–O(1B)	88.7(2)	O(1B)–Cu(1B)–N(1B)	91.7(2)

Table 4. Distances [Å] and angles [°] related to hydrogen bonding interactions in complexes 1 and 2 and CAH··· g and g··· g interactions in 3a.

D–H···A	[Å] D–H	[Å] H···A	[Å] D···A	[°] >D–H···A	Symmetry
1					
O(9)–H(9O)···O(5)	0.84	2.39	3.064(8)	138	1 − x, 1 − y, 1 − z
C(8)–H(8)···O(3)	0.95	2.59	3.269(9)	128	−1 + x, y, z
2					
C(4)–H(4)···O(6)	0.95	2.49	3.327(3)	146	1 + x, y, z
C(7)–H(7A)···O(9)	0.99	2.54	3.053(3)	112	1 + x, −1 + y, z
C(7)–H(7B)···O(3)	0.99	2.52	3.217(3)	127	3 − x, −y, 2 − z
C(14)–H(14A)···O(2)	0.99	2.55	3.300(2)	133	x, y, −1 + z
C(14)–H(14B)···O(10)	0.99	2.50	3.395(3)	150	x, ½ − y, ½ + z
C(18)–H(18A)···O(10)	0.98	2.46	3.225(3)	135	1 − x, 1 − y, 1 − z
3a					
C(12B)–H(12B)···n^1	0.95	3.00	3.836(3)	148	1 − x, 1 − y, 1 − z
n···n^2			3.623(5)	88.9(4)	

1 : Cg (centroid: C26 C27 C28 C23 C24 C25); 2: Cg (C19A C20A C21A N1A C17A C18A)···Cg (C21B N1B C17B C18B C19B C20B).

Table 5. Crystallographic data for 1–3a.

	1	2	3a
Empirical formula	$C_{34}H_{28}Cu_2O_{18}$	$C_{40}H_{44}Cu_2O_{20}S_4$	$C_{114.5}H_{86}Cu_4N_4O_{25.5}$
Formula weigh	851.64	1100.07	2350.11
T (K)	100(2)	100(2)	100(2)
Wavelength (Å)	0.71073	0.71073	0.71073
System, space group	triclinic, $P\bar{1}$	triclinic, $P\bar{1}$	triclinic, $P\bar{1}$
Unit cell dimensions			
a (Å)	6.9515(13)	9.7118(5)	11.9154(9)
b (Å)	10.484(2)	11.5379(6)	12.2788(10)
c (Å)	11.897(2)	11.7398(6)	20.7316(17)
α (°)	89.217(10)	68.278(2)	79.572(2)
β (°)	76.633(10)	68.196(2)	76.571(2)
γ (°)	82.988(11)	70.222(2)	86.476(2)
V (Å^3)	837.2(3)	1103.44(10)	2900.9(4)
Z	1	1	1
D_{calc} (g cm^{-3})	1.689	1.655	1.345
μ (mm^{-1})	1.356	1.235	0.804
$F(000)$	434	566	1211
Crystal size (mm)	0.285 × 0.056 × 0.040	0.149 × 0.141 × 0.091	0.192 × 0.164 × 0.085
hkl ranges	$-7 \le h \le 7$ $-11 \le k \le 11$ $-13 \le l \le 13$	$-14 \le h \le 14$ $-16 \le k \le 16$ $-17 \le l \le 17$	$-13 \le h \le 13$ $-14 \le k \le 13$ $-23 \le l \le 23$
2θ range (°)	2.613 to 23.314	2.323 to 31.581	2.225 to 23.943
Reflections collected/unique/[R_{int}]	6740/2312/[R_{int}] = 0.1019	42882/7357/[R_{int}] = 0.0440	75981/8998/[R_{int}] = 0.0929
Completeness to θ	95.1% (23.314°)	99.5% (25.242°)	99.4% (23.943°)
Absorption correction	Semi-empirical	Semi-empirical	Semi-empirical
Maximum and minimum transmission	0.7449 and 0.6029	0.7462 and 0.6941	0.7450 and 0.6700
Refinement method	Full matrix least-squares on F^2	Full matrix least-squares on F^2	Full matrix least-squares on F^2
Data/restrains/parameters	2312/0/244	7357/0/302	8988/5/727
Goodness of fit (GOF) on F^2	0.976	1.053	1.031
Final R indices [$I > 2\sigma(I)$]	R_1 = 0.0575, wR_2 = 0.1212	R_1 = 0.0353, wR_2 = 0.0728	R_1 = 0.0737, wR_2 = 0.1965
R indices (all data)	R_1 = 0.1103 wR_2 = 0.1429	R_1 = 0.0526 wR_2 = 0.0777	R_1 = 0.1162 wR_2 = 0.2256
Extinction coefficient	n/a	n/a	n/a
Largest Difference in peak and hole (e Å^{-3})	0.555 and −0.712	1.395 and −0.661	1.442 and −0.628